Pergamon

Geochimica et Cosmochimica Acta, Vol. 65, No. 2, pp. 223–235, 2001

0016-7037/01 $20.00 + .00

PII S0016-7037(00)00537-8

Iron sulfides and sulfur species produced at hematite surfaces in the presence of sulfate-reducing bacteria

ANDREW L. NEAL[1,*] SOMKIET TECHKARNJANARUK[1,†] ALICE DOHNALKOVA,[2] DAVID MCCREADY,[2] BRENT M. PEYTON,[3] and GILL G. GEESEY[1,4]

[1]Center for Biofilm Engineering, Montana State University, Bozeman, MT 59717, USA
[2] Environmental Molecular Sciences Laboratory, Pacific Northwest National Laboratory, Richland, WA 99352, USA
[3]Center for Multiphase Environmental Research, Washington State University, Pullman, WA 99164, USA
[4]Department of Microbiology, Montana State University, Bozeman, MT 59717, USA

(*Received March* 6, 2000; *accepted in revised form August* 11, 2000)

Abstract—In the presence of sulfate-reducing bacteria (*Desulfovibrio desulfuricans*) hematite (α-Fe_2O_3) dissolution is affected potentially by a combination of enzymatic (hydrogenase) reduction and hydrogen sulfide oxidation. As a consequence, ferrous ions are free to react with excess H_2S to form insoluble ferrous sulfides. X-ray photoelectron spectra indicate binding energies similar to ferrous sulfides having pyrrhotite-like structures (Fe2$p_{3/2}$ 708.4 eV; S2$p_{3/2}$ 161.5 eV). Other sulfur species identified at the surface include sulfate, sulfite and polysulfides. Thin film X-ray diffraction identifies a limited number of peaks, the principal one of which may be assigned to the hexagonal pyrrhotite (102) peak (d = 2.09 Å; 2θ = 43.22°), at the hematite surface within 3 months exposure to sulfate-reducing bacteria (SRB). High-resolution transmission electron microscopy identifies the presence of a hexagonal structure associated with observed crystallites. Although none of the analytical techniques employed provide unequivocal evidence as to the nature of the ferrous sulfide formed in the presence of SRB at hematite surfaces, we conclude from the available evidence that a pyrrhotite stiochiometry and structure is the best description of the sulfides we observe. Such ferrous sulfide production is inconsistent with previous reports in which mackinawite and greigite were products of biological sulfate reduction (Rickard 1969a; Herbert et al., 1998; Benning et al., 1999). The apparent differences in stoichiometry may be related to sulfide activity at the mineral surface, controlled in part by H_2S autooxidation in the presence of iron oxides. Due to the relative stability of pyrrhotite at low temperatures, ferrous sulfide dissolution is likely to be reduced compared to the more commonly observed products of SRB activity. Additionally, biogenic pyrrhotite formation will also have implications for geomagnetic field behavior of sediments. *Copyright © 2001 Elsevier Science Ltd*

1. INTRODUCTION

Any sulfur compound with an oxidation state greater than S^{2-} (i.e., S^0, S^{4+} and S^{6+}) has the potential to act as terminal electron acceptor in biologic oxidation of organic compounds (Goldhaber and Kaplan, 1974). Whilst assimilatory sulfate-reduction is commonplace, dissimilatory sulfate-reduction is carried out by a specialized group of nutritionally diverse organisms known collectively as anaerobic sulfate-reducing bacteria (SRB), including the genus *Desulfovibrio*. The observed activity of SRB in diverse habitats, including freshwater (Smith and Klug, 1981) and marine (Jørgensen, 1977) sediments, subsurface aquifers (Olson et al., 1981) and hydrothermal vent systems (Baross and Deming, 1983) points to their environmental significance.

The geological significance of SRB activity derives from the production of H_2S, resultant from sulfate-reduction, and its subsequent reaction with Fe^{2+} (the most abundant sulfide binding ion in typical reducing sediments) to form ferrous sulfides. Such sulfides are common components of both recent and ancient sediments and include the tetragonal, sulfur-deficient Fe^{2+}-sulfide, mackinawite (FeS-$Fe_{1.07}S$, Lennie et al., 1995a), the mixed-valence thiospinel, greigite (Fe_2^{3+}, Fe^{2+} S_4, Vaughan and Ridout, 1971) and the Fe^{2+}-polysulfide, pyrite (FeS_2). Iron sulfide mineral formation can be significant, annually an estimated 3.9×10^{13} g of pyrite-S are deposited in deltaic and anoxic continental shelf sediments (Berner, 1982). Sulfide production by SRB also has implications for steel corrosion (Hamilton, 1991) and bioremediation of heavy metal pollution in anoxic environments (Miller, 1950; Bacon et al., 1980; Webb et al., 1998).

Ferrous sulfides resulting from SRB activity have been studied previously and described as mackinawite and/or greigite (Rickard, 1969a; Herbert et al., 1998; Benning et al., 1999). In the aforementioned studies, ferrous sulfides were produced by free-living bacteria in liquid culture with added ferrous ions. However, most subsurface bacterial activity is likely to be associated with surfaces (Ghiorse and Wilson, 1988; Costerton et al., 1995), for example, the majority (98%) of bacteria in a Cape Cod aquifer were found to be attached (Harvey et al., 1984). We have therefore chosen to study ferrous sulfide production by bacteria associated with hematite surfaces.

In this study we identify ferrous sulfides produced by *Desulfovibrio desulfuricans* associated with hematite (α-Fe_2O_3) surfaces. The iron oxides goethite, lepidocrocite, ferrihydrite

*Author to whom correspondence should be addressed (andy_n@erc.montana.edu).
† *Present address:* Biochemical Engineering and Pilot Plant Research and Development Unit, National Center for Genetic Engineering and Biotechnology, Pilot Plant Development and Training Institute, King Mongkut University of Technology, Thouburi Thakham, Baugkhuntien, Bangkok, Thailand 10150.

and hematite are important Fe(III)-containing constituents of soils and sediments (Appelo and Postma 1996). The specular hematite used for these experiments lends itself to manipulation both during bacterial culture and subsequent chemical analysis. Dissimilatory bacterial sulfate reduction, using lactate as the electron donor, is described in Eqn. 1 (Thauer et al., 1977),

$$2\ \text{Lactate} + SO_4^{2-} + H^+ \rightarrow 2\ \text{Acetate} + 2CO_2 + 2H_2O + HS^- . \quad (1)$$

With no ferrous salts added to the growth medium, aq. [Fe^{2+}] is potentially dependent upon a combination of indirect (*sensu.* Brown et al. 1999) reductive dissolution of hematite by hydrogen sulfide analogous to generalized goethite dissolution (Eqn. 2, Pyzik and Sommer, 1981);

$$8Fe_2O_3 + 8H_2S + 32H^+ \rightarrow 16Fe^{2+}_{(aq.)} + S_8^0 + 24H_2O \quad (2)$$

and direct reduction due to cell associated hydrogenase activity (Eqn. 3, Robert and Berthelin 1986; Le Gall et al., 1994)

$$Fe_2O_3 + 6H^+ + 2e^- \rightarrow 2Fe^{2+}_{(aq.)} + 3H_2O. \quad (3)$$

With the aim of investigating ferrous sulfide chemistry resulting from SRB activity at iron oxide surfaces (as opposed to liquid culture) we present X-ray photoelectron spectroscopic, X-ray diffraction and transmission electron microscopic evidence that the ferrous sulfides differ from those phases previously identified (i.e., mackinawite and greigite). Although an unequivocal assignment is insoluble, the techniques suggest that the surface associated precipitates are best described as pyrrhotite-like.

2. METHODS

2.1. Organisms and Culture

Two *Desulfovibrio desulfuricans* strains were used in the experiments described here, G20 and Essex 6 (ATCC 29577, NCIMB 8307, Postgate and Campbell, 1966). G20 was derived from *D. desulfuricans* G100A (Wall et al., 1993). Both strains were a gift of Dr. J. Wall, University of Missouri. A green fluorescent protein (GFP) reporter gene construct was used to visualize cells of *D. desulfuricans* strain G20. In our laboratory, the *IncQ* plasmid pdsk519 encoding for GFP-*mut2* (Matthysse et al., 1996) was modified for chloramphenicol resistance and mobilized into G20 with GFP expression under control of the constitutive *npt2* promoter. The *mut2* derivative of the wild type GFP gene confers a 30-fold increase in chromophore fluorescence intensity (Cormack et al., 1996). Use of such recombinant organisms allows in situ, non-destructive visualization of bacteria at surfaces avoiding artifacts such as changes in surface chemistry caused by more traditional staining methods (e.g., DAPI, see review by Errampalli et al., 1999).

D. desulfuricans, a facultative anaerobe, was grown in batch culture in 25 mL anaerobic serum bottles with butyl rubber septa and aluminum crimp caps (Wheaton, Millville, NJ) in Lactate Medium C (Butlin et al., 1949; Postgate, 1963). Lactate Medium C contains 8 ml l^{-1} 60% sodium lactate syrup, 4.5 g l^{-1} Na_2SO_4, 2 g l^{-1} $MgSO_4$, 1 g l^{-1} yeast extract, 1 g l^{-1} NH_4Cl, 0.5 g l^{-1} K_2HPO_4 and 0.06 g l^{-1} $CaCl_2$ ($\Sigma[SO_4^{2-}]$ = 40 mM) in distilled, deionized water and adjusted to pH 7 with 6N NaOH. Na-thioglycollate ($C_2H_3O_2SNa$) and ascorbic acid were added at a concentration of 0.01 g l^{-1} to poise E_h of the medium at circa. −100 mV. All media was sterilized by autoclave at 121°C for 20 min. The medium was supplemented with chloramphenicol (20 μg ml^{-1}) to maintain selective pressure for plasmid retention by the cells. *D. desulfuricans* Essex 6 was also grown in the absence of SO_4^{2-} employing pyruvate fermentation with fumarate as the electron acceptor (Postgate and Campbell, 1966; Magee et al., 1978). The medium contains 4.5 g l^{-1} Na-fumarate (35 mM), 3.5 g l^{-1} Na-pyruvate (34 mM), 1.6 g l^{-1} $MgCl_2$, 1 g l^{-1} NH_4Cl, 1 g l^{-1} yeast extract, 0.5 g l^{-1} KH_2PO_4 and 0.1 g l^{-1} $CaCl_2$ (pH 7). Reductants were again added to poise medium E_h. Preliminary experiments have demonstrated that Essex 6 is unable to couple the oxidation of pyruvate to thioglycollate reduction. Thus the effect of *D. desulfuricans* presence at the hematite surface in the absence of sulfate (and therefore H_2S), could be assessed.

2.2. Materials and Experimentation

Natural specular hematite (α-Fe_2O_3) from Bahia, Brazil was used for this study, a gift of Dr. K. Rosso (Pacific Northwest National Laboratory, Richland, WA). Hematite samples (dimensions approximately 5 × 3 × 0.2 mm) were washed before use in distilled, deionised water to remove particulate surface contamination.

The potential reductive effect of Na-thioglycollate and ascorbic acid as well as any possible photoreduction of hematite in the medium was evaluated by incubating a hematite sample in Lactate Medium C without the addition of bacteria for seventeen days at room temperature (23–26°C). Additionally samples were exposed to Lactate Medium C in the presence of G20 or Essex 6 for 17 d and to Essex 6 for three months. Other treatments included Essex 6 in sulfate-free medium and Lactate medium C in the absence of bacteria but with the addition of approximately 150 μM H_2S. Hematite samples were added to serum bottles before autoclaving. Following incubation, hematite samples with associated precipitates were removed from the culture medium and observed using epifluorescent microscopy to evaluate the presence/absence of SRB, after which they were washed in O_2-free distilled, deionised water and dried under a stream of N_2 before being mounted and placed in the XPS vacuum chamber.

2.3. Instrumentation

2.3.1. Optical microscopy

Observation of bacteria attached to the hematite surface was made using an Olympus BX60 microscope equipped with an infinity-corrected, long working distance water immersion objective lens (40×, NA = 0.55, Nikon Inc., Torrence, CA) and 100 W Hg-vapor discharge lamp. Reflected differential interference contrast (DIC) images were captured using a U-DICR polarizer (Olympus America Inc., Lake Success, NY), fluorescence images with a WIBA filter block (460–490 nm excitation; 505 nm dichroic mirror; 515–550 nm emission; Olympus America Inc.). Video capture was performed using an ImagePoint™ monochrome, Peltier cooled (+10 °C) CCD camera (Photometrics Ltd., Tuscon, AZ) and Image-Pro Plus™ software (Media Cybernetics, Silver Springs, MD).

2.3.2. X-ray photoelectron spectroscopy

X-ray photoelectron spectroscopy (XPS) was performed on a Model 5600ci spectrometer (Perkin Elmer Inc., Eden Prairie, MN). The instrument was calibrated employing the Au4$f_{7/2}$, Cu2$p_{3/2}$ and Ag3$d_{5/2}$ photopeaks with binding energies of 83.99, 932.66 and 368.27 eV respectively. A 5 eV flood gun was used to offset charge accumulation on the samples. A consistent 800 μm diameter area was analyzed on all surfaces using a monochromatized AlK_α X-ray source (1486.6 eV) at 300 W and a pass energy of 93.9 eV for broad scans, 29.35 eV for high-resolution scans (nominal resolution = 0.3 eV). The system was operated at a base pressure of 10^{-8}–10^{-9} τ. To correct for sample charging, all reported literature-based binding energies have been referenced to the adventitious C1*s* peak observed on hematite exposed to Lactate Medium C in the absence of bacteria at 285.1 eV.

Fe2$p_{3/2}$ spectra were analyzed using a multiplet splitting model derived from consideration of electrostatic and spin-orbit interactions (Gupta and Sen, 1974; Gupta and Sen, 1975). We have however followed the practice of McIntyre and Zetaruk (1977), Pratt et al. (1994a) and Pratt et al. (1994b) in fitting only three major peaks to the Fe^{2+}-S spectrum, ignoring two minor peaks at elevated binding energies (E_b). Fe^{3+}-O spectra have been fitted using four peaks, consistent with the aforementioned authors. S2*p* spectra have been fitted employing asymmetric doublets (ΔE_b 1.18 eV) reflecting the spin-orbit splitting of S2$p_{3/2}$ and S2$p_{1/2}$ photopeaks. Following baseline subtraction (Shirley, 1972), curves were fit employing combinations of Lorenztian

Table 1. XPS reference binding energies of iron and sulfur species encountered at the hematite surface.

Species	Mineral	Binding energy (eV)[a]	FWHM[b] (eV)	Reference
Fe2$p_{3/2}$				
Fe^{3+}-O	hematite (α–Fe_2O_3)	711.1		McIntyre and Zetaruk, 1977
		711.3		Junta-Rosso and Hochella, 1996
		711.0		Asami et al., 1976
Fe^{2+}-S	pyrrhotite ($Fe_{0.89}S$)	708.5		Buckley and Woods, 1985
	pyrrhotite (Fe_7S_8)	707.8	2.3	Jones et al., 1992
		707.6	1.6	Pratt et al., 1994b
		707.5	1.6	Pratt et al., 1994a
	greigite (Fe_2^{3+}, $Fe^{2+}S_4$)	707.3	1.6	Herbert et al., 1998
	mackinawite ($Fe_{1+x}S$)	707.8		Lennie and Vaughan, 1996
	pyrite (FeS_2)	707.5		Buckley and Woods, 1987
Fe^{3+}-S	pyrrhotite (Fe_7S_8)	708.9	1.3	Pratt et al., 1994b
		709.3		Pratt et al., 1994a
	greigite (Fe_2^{3+}, Fe^{2+} S_4)	709.2	1.4	Herbert et al., 1998
S2p				
S^{2-}	greigite (Fe_2^{3+}, Fe^{2+} S_4)	161.0	1.3	Herbert et al., 1998
	pyrrhotite ($Fe_{0.89}S$)	161.6		Buckley and Woods, 1985
	pyrrhotite (Fe_7S_8)	161.4	1.9	Jones et al., 1992
		161.3	0.9–1.2	Pratt et al., 1994a
		161.3	1.3	Pratt et al., 1994b
	mackinawite ($Fe_{1+x}S$)	162.4		Lennie and Vaughan, 1996
	pyrite (FeS_2)	162.8		Buckley and Woods, 1987
S_2^{2-}		162.5		Mycroft et al., 1990
		162.3	1.3	Pratt et al., 1994b
S_n^{2-}		163.8		Hyland and Bancroft, 1989
		163.3	0.9–1.2	Pratt et al., 1994a
		163.3	2.2	Pratt et al., 1994b
$S_2O_3^{2-}$		164.0		Manocha and Park, 1977
		164.0	1.3	Pratt et al., 1994b
S^0		164.4	0.9–1.2	Pratt et al., 1994a
		164.2		Hyland and Bancroft, 1989
SO_3^{2-}		166.5		Wagner et al., 1992
		166.5	0.9–1.2	Pratt et al., 1994a
SO_4^{2-}		168.3	0.9–1.2	Pratt et al., 1994a
		168.6	1.4	Pratt et al., 1994b
		168.8	2.0	Jones et al., 1992
$S_2O_3^{2-}$		169.7		Manocha and Park, 1977

[a] All E_b are referenced to a C1s of 285.1 eV
[b] Full width at half maximum

and Gaussian line shapes. Table 1 contains Fe2$p_{3/2}$ and S2p E_b from previous studies, referenced to the adventitious C1s of 285.1 eV.

2.3.3. X-ray diffraction

Thin film X-ray diffraction was carried out on precipitates at the hematite surface using a Phillips X'Pert MPD (Phillips Analytical, Natick, MA) incorporating a vertical theta-theta goniometer (220 mm radius) and a long fine focus ceramic X-ray tube with a Cu anode. The instrument was operated at a power of 40 kV, 50 mA, using CuK_α radiation (λ = 1.541 Å). Parallel beam optics were employed with a Gutmann mirror providing a high intensity, parallel collimated incident beam. The receiving optics comprised a 0.09 radian parallel plate collimator and proportional counter detector. The sample was mounted at room temperature on an Anton-Paar TTK 450 thin-film stage under vacuum ($\sim 2 \times 10^{-2}$ τ). Diffractograms were run over the 2θ range 5°–75° with a (constant) angle of incidence (Ω) of 2.5°. Diffraction pattern analysis was performed using Jade 5™ software (Materials Data Inc., Livermore, CA) with comparison to the Joint Committee on Powder Diffraction Standards (JCPDS) database.

2.3.4. High resolution TEM (HR-TEM)

Hematite samples with associated precipitates were anaerobically embedded in hard grade LR White™ resin, and cured for six hours at 60°C. Hardened blocks were sectioned in an anaerobic glove box using a Leica UltraCut R microtome (Leica Microsystems Inc., Deerfield, IL). In an attempt to minimize sample compression and hematite fracture during sectioning, a Diatome Ultra 35° knife was used in favor of the more common 45° knife (see Jesior 1986). The lower angle edge resulted in sections without hematite fracture of sufficient area to investigate the attached biofilm precipitates. Fifty nanometer thick sections were collected at room temperature on copper grids supported with lacey carbon film and observed at 200 kV using a JEOL 2010 high-resolution analytical electron microscope (JEOL USA Inc., Peabody, MA). High-resolution images were collected and analyzed by DigitalMicrograph® 3 software (Gatan Inc., Pleasanton, CA).

3. RESULTS

3.1. Evaluation of Culture Medium and Bacteria Attached to Hematite

Throughout incubation, culture media were visually evaluated for the formation of ferrous sulfides in suspension as a black discoloration of the normally straw-colored (due to the inclusion of yeast extract in the medium) solution. In no treatment was such discoloration observed, suggesting that if any ferrous sulfide production had taken place it was confined to the hematite surfaces. Epifluorescent microscopic observation con-

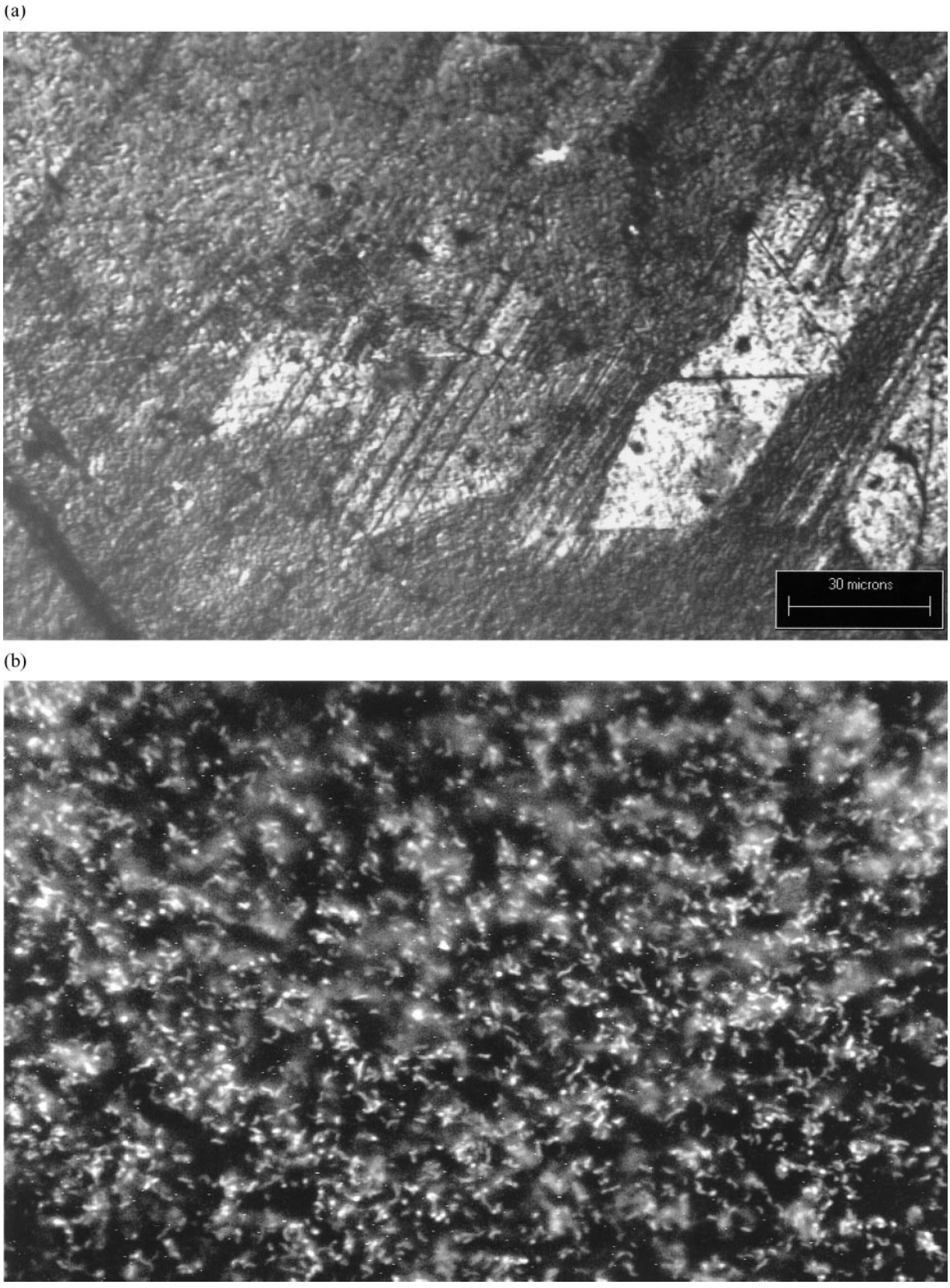

Fig. 1. Reflected DIC (above) and corresponding epifluorescence (below) photomicrographs of *Desulfovibrio desulfuricans* G20 (pNpt2CmGFP) attached to a hematite surface after 17 d in culture. The scale bar associated with the DIC image is representative of both images. 40× long working distance, water immersion lens. DIC image, 32 msec exposure, 4 dB gain, Epifluorescent image, 10 sec exposure, 4 dB gain.

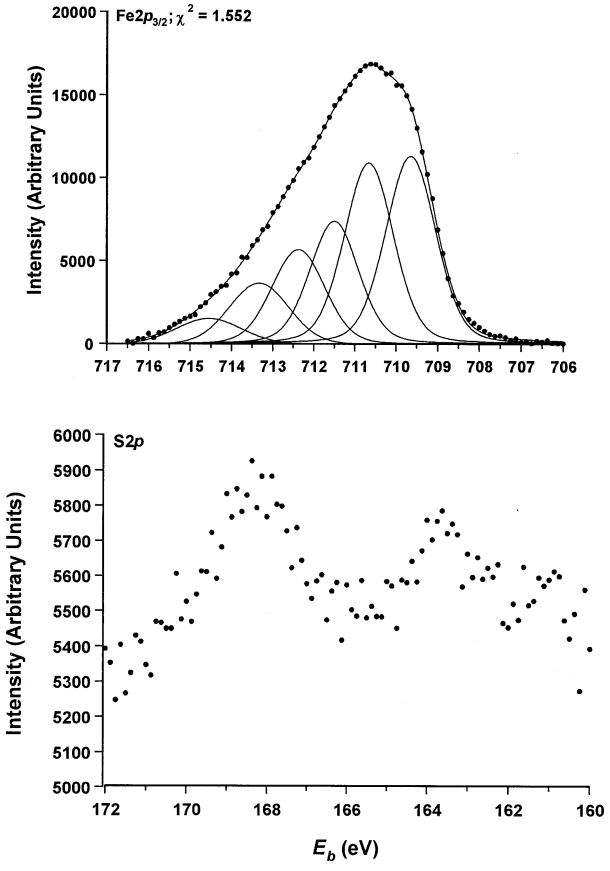

Fig. 2. XPS spectra of hematite surface exposed to growth medium in the absence of sulfate-reducing bacteria. Fe2$p_{3/2}$; component photopeaks are fitted representing Fe^{3+}-O of the hematite surface, the peak weighted average is 710.9 eV. S2*p*; despite the low signal to noise ratio, photopeaks representative of sulfate (*circa.* 168 eV), elemental sulfur/thiosulfate (*circa.* 164 eV) can be distinguished. Component bands were fitted to the Fe2$p_{3/2}$ spectrum following baseline subtraction (see Section 2.3 for details on baseline substraction and curve fitting). Adventitious C1s = 285.1 eV.

firmed the association of *D. desulfuricans* with the precipitates formed at the mineral surfaces (Fig. 1). No bacteria were observed on sterile mineral surfaces.

3.2. XPS Spectra of Hematite Surfaces

3.2.1. Sterile hematite surface

The presence of adventitious C and N was observed on the hematite surface, no doubt resulting from exposure to the growth medium but also potentially, from fluid infiltration between adjacent hematite platelets in the original hematite crystal (Junta-Rosso and Hochella, 1996). The Fe2$p_{3/2}$ region is shown in Figure 2 together with the results of curve fitting. In accordance with McIntyre and Zetaruk (1977) a pair of narrow photopeaks separated by 1.2 eV best fit the steep leading edge of the Fe2*p* region (χ^2 = 1.55). The Fe^{3+}-O peak weighted average is 710.9 eV, consistent with published hematite XPS spectra (Asami et al., 1976; McIntyre and Zetaruk, 1977; Junta-Rosso and Hochella, 1996). A photopeak in the O1*s* core region at 529.9 eV was attributed to O^{2-} of hematite (Junta-Rosso and Hochella, 1996, data not shown). Although at every step of sample preparation care was taken to avoid sample oxidation, assessment of the degree of oxidation (if any) was not possible because precipitates were analyzed in situ at the hematite surface and the O^{2-} photopeak of the substratum confounds the identification of oxidized species potentially associated with precipitates. Since the primary product of SRB activity on the hematite surface was expected to be ferrous sulfide, the S2*p* region was also studied on the unexposed surface. Despite a low signal-to-noise ratio, weak photopeaks were observed at circa 164 eV, 168 eV and at 161 eV (Fig. 2). These photopeaks can be attributed to $S_8^0/S_2O_3^{2-}$ (Hyland and Bancroft, 1989, Manocha and Park, 1977) and SO_4^{2-} (Jones et al., 1992) and S^{2-} (Buckley and Woods, 1985; Pratt et al., 1994a,b) species respectively, presumably resulting from sulfate adsorption from the growth medium and the reductive effect of medium associated Na-thioglycollate both on the hematite surface and sulfate. Some reduction and sulfide formation therefore occurs in the absence of bacteria however, as will be demonstrated, the degree of reduction is inconsequential relative to reduction and sulfide production in the presence of SRB.

3.2.2. Hydrogen sulfide exposed hematite surface

The Fe2$p_{3/2}$ region exhibited a contribution at low E_b indicative of Fe^{2+} (Fig. 3). Curve fitting employed the hematite model established from the unexposed surface (Fe^{3+}-O, see Fig. 2), with the addition of a principal photopeak at 708.7 eV (FWHM = 1.4 eV) and two multiplets 0.9 eV either side of the major peak (χ^2 = 1.24, see Fig. 3). The E_b of the principal peak is in good agreement with the Fe2$p_{3/2}$ Fe^{2+}-S photopeak collected on pyrrhotite by Buckley and Woods (1985, see Table 1). Since the Fe^{3+}-S component of the putative pyrrhotite (Pratt et al., 1994a,b) is likely to be confounded with the Fe^{3+}-O component of hematite, whilst accepting the lack of adherence to the pyrrhotite model, no attempt was made to include these photopeaks in the curve fitting procedure. Instead, corroborating evidence was sought in the S2*p* core region for the identification of the ferrous sulfide.

The S2*p* region is potentially complicated by contributions from monosulfide (S^{2-}), disulfide (S_2^{2-}) and polysulfide (S_n^{2-}) species (Hyland and Bancroft, 1989). S^{2-} and S_2^{2-} peaks originate from S-Fe bonds whilst S_n^{2-} peaks originate from S-S bonds. To obtain a good fit to the data (χ^2 = 1.33), we have adopted the approach of previous authors (Pratt et al. 1994a; Herbert et al., 1998) in fitting doublets (ΔE_b 1.18 eV) for S_2^{2-} and S_n^{2-} to the high E_b tail in the S2*p* core region. The principal S2$p_{3/2}$ photopeak was identified at 167.9 eV (FWHM = 1.3 eV) corresponding to SO_4^{2-}, undoubtedly likely due to adsorption of sulfate from the growth medium, accompanied by a second peak corresponding to SO_3^{2-} at 166 eV (FWHM = 1.3 eV) (Wagner et al., 1992). Minor photopeaks at 161.4 (FWHM = 1.3 eV) and 163.2 eV (FWHM = 1.2 eV) were ascribed to S^{2-} and S_2^{2-} respectively (Mycroft et al., 1990; Pratt et al., 1994a; Pratt et al., 1994b). Whilst the S^{2-} and S_2^{2-} may potentially be due to interactions with other cations in the growth medium (for example Mg^{2+} and Na^{2+}) the position of the monosulfide peak is again similar to pyrrhotite-like structures (Buckley and Woods, 1985; Jones et al., 1992; Pratt et al., 1994a; Pratt et al., 1994b).

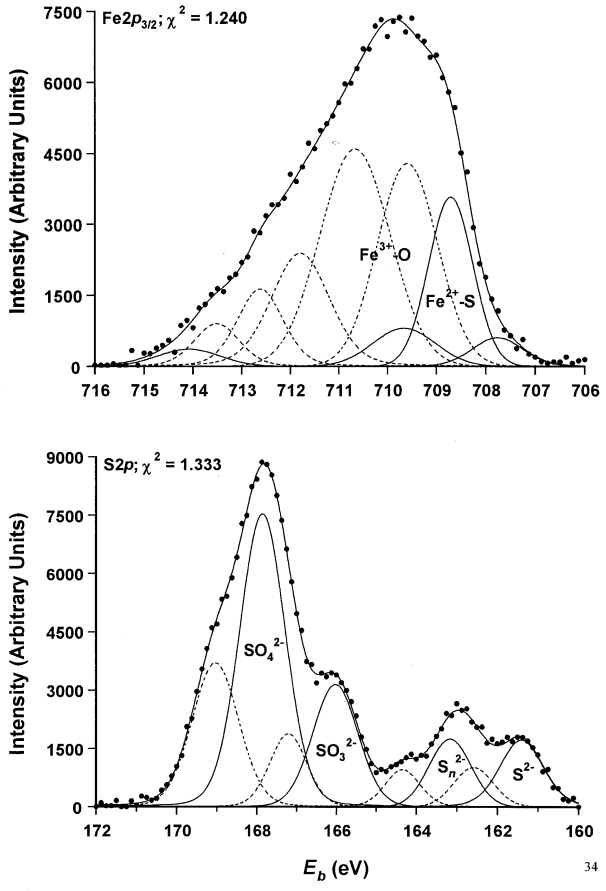

Fig. 3. XPS spectra of hematite surface exposed to hydrogen sulfide. Fe2$p_{3/2}$; Fe^{2+}-S contributions are indicated by solid lines, Fe^{3+}-O contributions by broken lines. The Fe^{2+}-S maximum is at 708.7 eV. S2*p*; S-species are represented by multiplet peaks representing the S2$p_{3/2}$ and S2$_{1/2}$ spin states, S2$p_{3/2}$ contributions for the S-species indicated are respented by solid lines, the corresponding S2$p_{1/2}$ contributions by broken lines. Component bands were fitted to both spectra following baseline subtraction. (See Section 2.3 for details on baseline subtraction and curve fitting). Adventitous Cls = 285.1 eV.

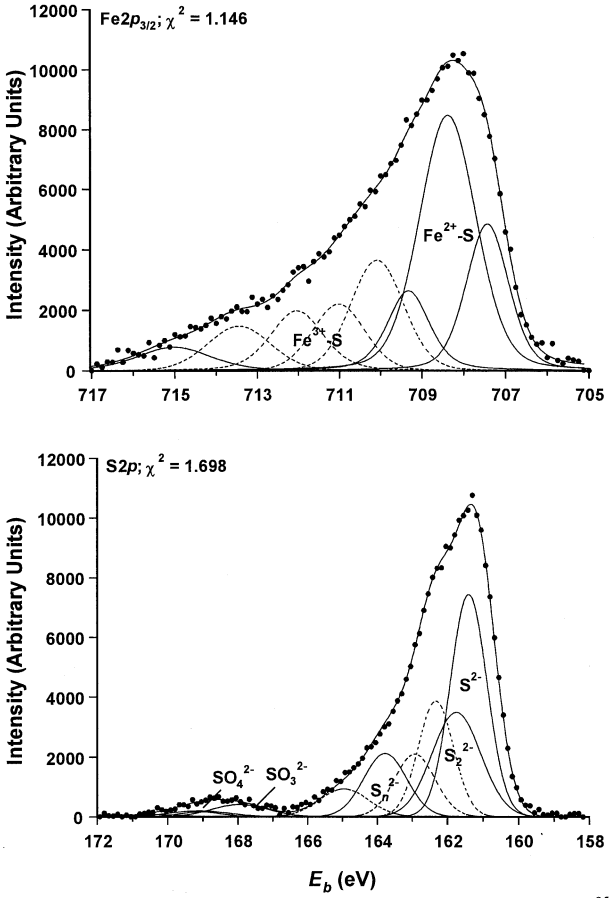

Fig. 4. XPS spectra of hematite sulface exposed to the sulfate-reducing bacterium *Desulfovibrio desulfuricans* Essex 6 for 17 d. Fe2$p_{3/2}$; Fe^{2+}-S contributions are indicated by solid lines, Fe^{3+}-S contributions by broken lines. The Fe^{2+}-S maximum is at 708.4 eV. S2*p*; S-species are represented by multiplet peaks representing the S2$p_{3/2}$ and S2$p_{1/2}$ spin states, S2$p_{3/2}$ contribution for the S-species indicated are represented by solid lines, the corresponding S2$p_{1/2}$ contributions by broken lines. Component bands were fitted to both spectra following baseline subtraction. (See Section 2.3 for details on baseline subtraction and curve fitting). Adventitious C1s = 285.1 eV.

3.2.3. SRB exposed hematite surface

Broad scan spectra (not shown) suggested C1*s* and N1*s* peak intensities were increased (relative to O1*s*) on all hematite surfaces exposed to *D. desulfuricans* (compared to unexposed surfaces) and a prominent photopeak was present in the C1*s* core region at ~288 eV. Such surface differences can be accounted for by, among other things, organic species associated with bacteria (i.e., proteins, lipids, polysaccharides etc., see Rouxhet and Genet, 1991).

The XPS spectra of the hematite surface exposed to Essex 6 in the presence of sulfate suggested that the sulfide layer was of sufficient thickness to mask any hematite-related signal (see Fig. 4). The Fe^{2+}-S photopeak was identified at 708.4 eV (FWHM = 1.5 eV, $\chi^2 = 1.15$). In the S2*p* region, the S^{2-} peak was identified at 161.3 eV (FWHM = 1.6 eV), the S_2^{2-} peak at 162.5 eV (FWHM = 1.3 eV), S_n^{2-} at 163.9 eV (FWHM = 1.4 eV) and SO_4^{2-} at 168 eV (FWHM = 1.4 eV, $\chi^2 = 2.63$).

The Fe2*p* spectrum of G20 exposed hematite exhibited a shoulder at low E_b, the position of which was determined at 708.4 eV (FWHM = 1.4 eV, $\chi^2 = 1.72$). In the S2*p* region, the monosulfide S2$p_{3/2}$ peak is at 161.5 eV (FWHM = 1.3 eV), the S2$p_{3/2}$ S_2^{2-} peak at 162.2 eV (FWHM = 1.3 eV) and the S2$p_{3/2}$ S_n^{2-} peak at 163.6 eV (FWHM = 1.9 eV). The high E_b region was resolved into two pairs of multiplets, the S2$p_{3/2}$ peaks being at 166.7 eV (FWHM = 1.7 eV) and 168 eV (FWHM = 1.8 eV). These peak positions were suggestive of SO_3^{2-} and SO_4^{2-} respectively.

Interestingly, the hematite surface exposed to Essex 6 in the absence of medium-SO_4^{2-} (but containing sodium thioglycollate as a reductant and hence a potential source of sulfur) indicated not only a lack of metal sulfide species but the presence of $S_8^0/S_2O_3^{2-}$ and S_n^{2-} (peak maxima ~164 and ~170 eV) and SO_4^{2-}/SO_3^{2-} (peak maximum ~169 eV, Fig. 5).

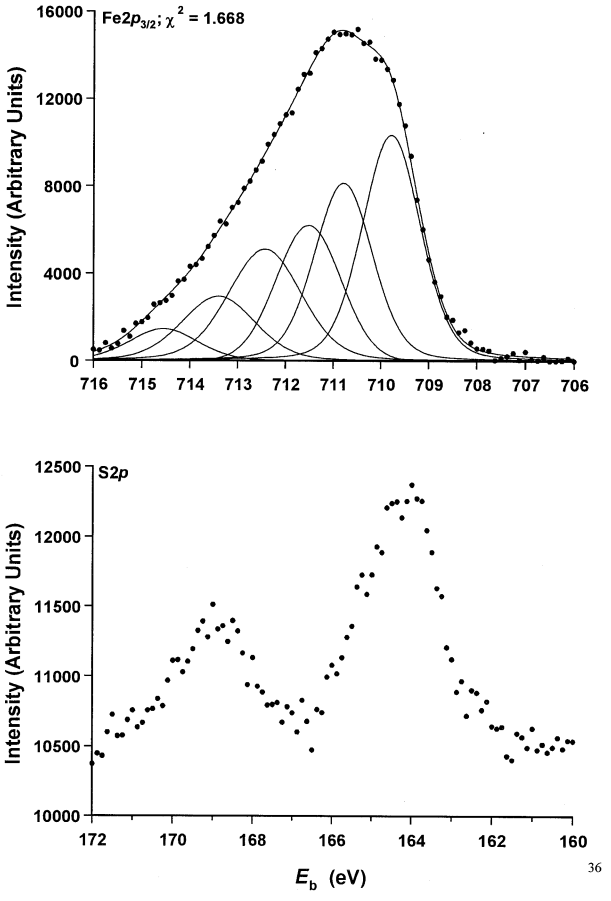

Fig. 5. XPS spectra of hematite surface exposed to Essex 6 in growth medium sulfate-lacking. Fe2$p_{3/2}$; the spectrum is suggestive of hematite Fe^{3+}-O, *cf.* Fig. 2. S2*p*; despite the low signal to noise ratio, photopeaks representative of elemental sulfur, thiosulfate can be distinguished. Adventitious C1s = 285.1 eV.

3.3. X-ray Diffraction of Precipitated Iron Sulfides

Thin film X-ray diffraction of precipitates on the hematite sample exposed to bacteria for 17 d indicated a broad peak at low angle suggestive of amorphous material and an absence of crystal structure associated with the precipitate. Following 3 months incubation in bacterial culture peaks were identified associated with precipitates on the hematite surface with *d*-spacings of 1.28, 1.81, 2.04 and 2.09 Å (2θ, 74.04°, 50.32°, 44.46° and 43.22° respectively, see Figure 6). The low number of peaks identified may result from a lack of heterogeneous orientation of the crystals at the hematite surface as well as the presence of small unobservable crystallites. With so few lines assignment of an unequivocal crystal structure is difficult, however the principal 2.09 Å (43.22° 2θ) peak may be assigned to the hexagonal pyrrhotite (102) peak (Lennie et al., 1995b). We remain cautious concerning this assignment however because minor peaks at such angles are a common feature of ferrous sulfides as well as S_8^0. Even so, XRD suggests that a crystal phase forms at the hematite surface in under three months.

3.4. HR-TEM of Precipitated Iron Sulfides

High magnification HR-TEM images of the hematite surface incubated for 3 months illustrate the presence of numerous crystals with regions of overgrowth (Fig. 7). Lattice spacings of 2.6, 3.8 and 5.1 Å were consistently measured for the observed crystals however, again unequivocal assignment to a particular phase was not possible. However, Fourier transformation of the 5.1 Å lattice spacing, the most commonly observed, yielded a hexagonal crystal structure (Fig. 8) adding weight to the identification of the ferrous sulfide phase as a putative pyrrhotite.

4. DISCUSSION

4.1. Ferrous Sulfide Production by Sulfate-Reducing Bacteria at Hematite Surfaces

The production of ferrous sulfides by SRB is dependent upon Fe^{2+} release from the hematite surface, affected potentially both by direct (i.e., hydrogenase) and indirect (i.e., H_2S oxidation) processes. Reaction between ferrous ions and excess H_2S subsequently results in ferrous sulfide production. Although none of the analytical techniques employed here (XPS, thin film XRD and HR-TEM) provide unequivocal evidence (either on their own or in combination) as to the nature of the ferrous sulfide formed in the presence of SRB at hematite surfaces, we conclude from the available evidence that a pyrrhotite stiochiomertry and structure is the best description of the sulfides we observe. This observation is at variance with previous studies of SRB ferrous sulfide production, although it is not without precedent; pyrrhotite is observed in anoxic marine sediments (Kobayashi and Nomura, 1972; Roberts and Turner, 1993; Horng et al., 1998) and at the surface of corroding iron and steel in H_2S-rich environments (Meyer et al., 1958; Berner, 1964; Ringas and Robinson, 1988). Moreover, low temperature pyrrhotite formation has been observed in laboratory studies (Berner, 1964; Sweeney and Kaplan, 1973).

The production of ferrous sulfides has long been used to identify SRB in mixed and single species culture (Butlin et al., 1949). Rickard (1969a) described the initial production of mackinawite and subsequently, greigite by *Desulfovibrio desulfuricans* Canet 41 in medium containing 182 mM $Fe^{2+}_{(aq.)}$. More recently, using a mixed bacterial culture and 14 μM $Fe^{2+}_{(aq.)}$, Herbert et al. (1998) have again identified mackinawite and greigite and Benning et al. (1999) have described mackinawite formation by *D. desulfuricans* ATCC 29578 (ferrous iron content unspecified). Magnetotactic bacteria, with close affiliations to SRB (DeLong et al., 1993), have been shown to produce intracellular mackinawite and greigite (Pósfai et al., 1998; Frankel et al., 1998; Schüler and Frankel, 1999).

Pyrite is understood to replace mackinawite by reaction between FeS and S_8^0 or S_n^{2-} (Berner 1964; Berner, 1970; Rickard 1969b; Taylor et al., 1979; Luther, 1991; Schoonen and Barnes, 1991b; Wilkin and Barnes, 1996; Benning et al., 2000) following the amorphous FeS $\rightarrow$ mackinawite $\rightarrow$ greigite $\rightarrow$ pyrite sequence. Previous studies have described little or no pyrite formation in SRB batch cultures despite significant accumulation of precursor ferrous sulfides (Rickard, 1969a; Herbert et al., 1998; Benning et al., 1999). An exception has been described by Donald and Southam (1999) who report that pyrite formation from FeS is accelerated in the presence of

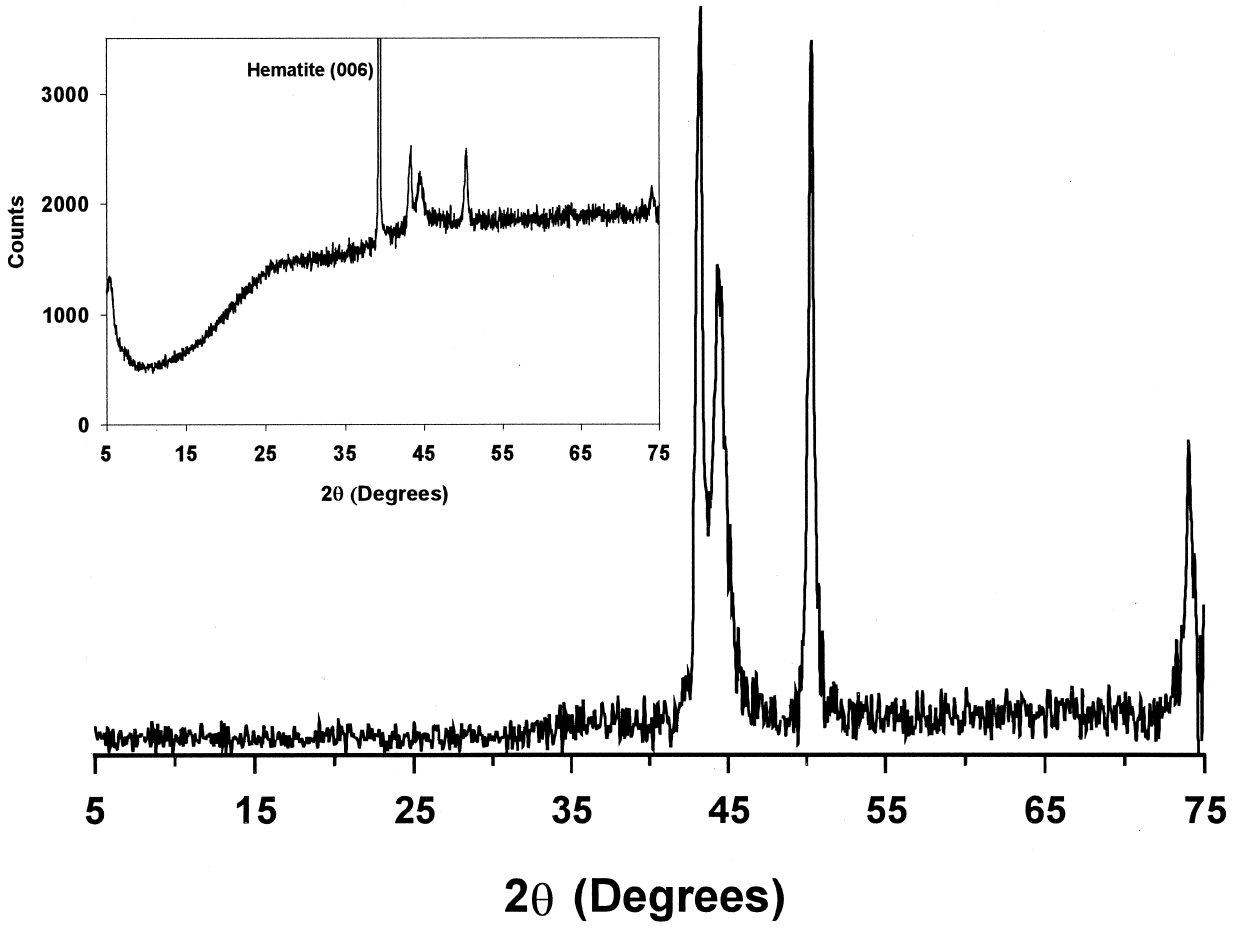

Fig. 6. Background subtracted XRD trace from the precipitate formed at a hematite surface in the presence of sulfate-reducing bacteria following 3 months of incubation. The hematite (006) peak has also been subtracted. Peaks are observed at 43.22° (d = 2.09Å), 44.46° (d = 2.04Å), 50.32° (d = 1.81Å) and 74.04° (d = 1.28Å). Inset—untransformed XRD trace indicating the relative intensities of the precipitate associated peaks compared to the hematite peak.

SRB, compared to abiotic processes, an apparent consequence of nucleation of pyrite on inner and outer surfaces of the cell envelope. However, despite the presence of oxidized sulfur species, in no instance was pyrite observed at the hematite surfaces in this study (FeS_2; Fe2$p_{3/2}$ 707.5 eV, S2$p_{3/2}$ 162.8 eV, Buckley and Woods, 1987). This fact may corroborate our identification of the ferrous sulfide as pyrrhotite since in the presence of oxidized sulfur species mackinawite and/or greigite, were they present, would be expected to transform to pyrite relatively quickly.

One significant difference between previous experiments and this study is the amount of $Fe^{2+}_{(aq.)}$ in the growth media. Whilst $SO^{2-}_{4(aq).}$ concentrations (and therefore likely subsequent H_2S concentrations) in the four studies range from 32 mM (Herbert et al., 1998) to 50 mM (Rickard, 1969a), $Fe^{2+}_{(aq.)}$ concentrations vary greatly between 182 mM (Rickard, 1969a) and an unknown but potentially low concentration in this study arising from the low dissolution rate of hematite (Byrne and Kester, 1976; dos Santos and Stumm, 1992). $Fe^{2+}_{(aq.)}$ supply could potentially play a role in determining the resultant ferrous sulfide stoichiometry. Thermodynamic calculations suggest the greigite stability field is particularly sensitive to changes in the $H_2S_{(aq.)}$: $Fe^{2+}_{(aq.)}$ ratio (Anderko and Shuler, 1997). Specifically, at a fixed Fe^{2+} molality of 10 mM kg^{-1}, greigite is not formed below 40 mM kg^{-1} H_2S (Anderko and Shuler, 1997). Berner (1971) also indicates that with sulfide activity (pS^{2-}) as the controlling factor the pyrrhotite stability field exists at lower pS^{2-} relative to pyrite (at equivalent E_h, see also Lord and Church, 1983). These sources place emphasis on pS^{2-} in determining the nature of the ferrous sulfide formed under particular circumstances, rather than the availability of ferrous ions. Since autooxidation of H_2S is likely to occur at the hematite surface (see dos Santos Afonso and Stumm, 1992; Herszage and dos Santos Afonso, 2000) the potential exists for pS^{2-} to be reduced in close proximity to the mineral surface. Visual inspection of the culture media indicates that ferrous sulfide formation is limited to the mineral surface—the very place where we might expected the most reduced pS^{2-}.

Alternatively the greigite stability field lies above the H^+/H_2 redox equilibrium, suggesting the mackinawite → greigite → pyrite sequence is thermodynamically unfeasible in strong reducing environments (Anderko and Shuler, 1997), indeed there is now considerable empirical evidence suggesting the conversion of mackinawite to pyrite requires an oxidant, i.e., S^0_8 or

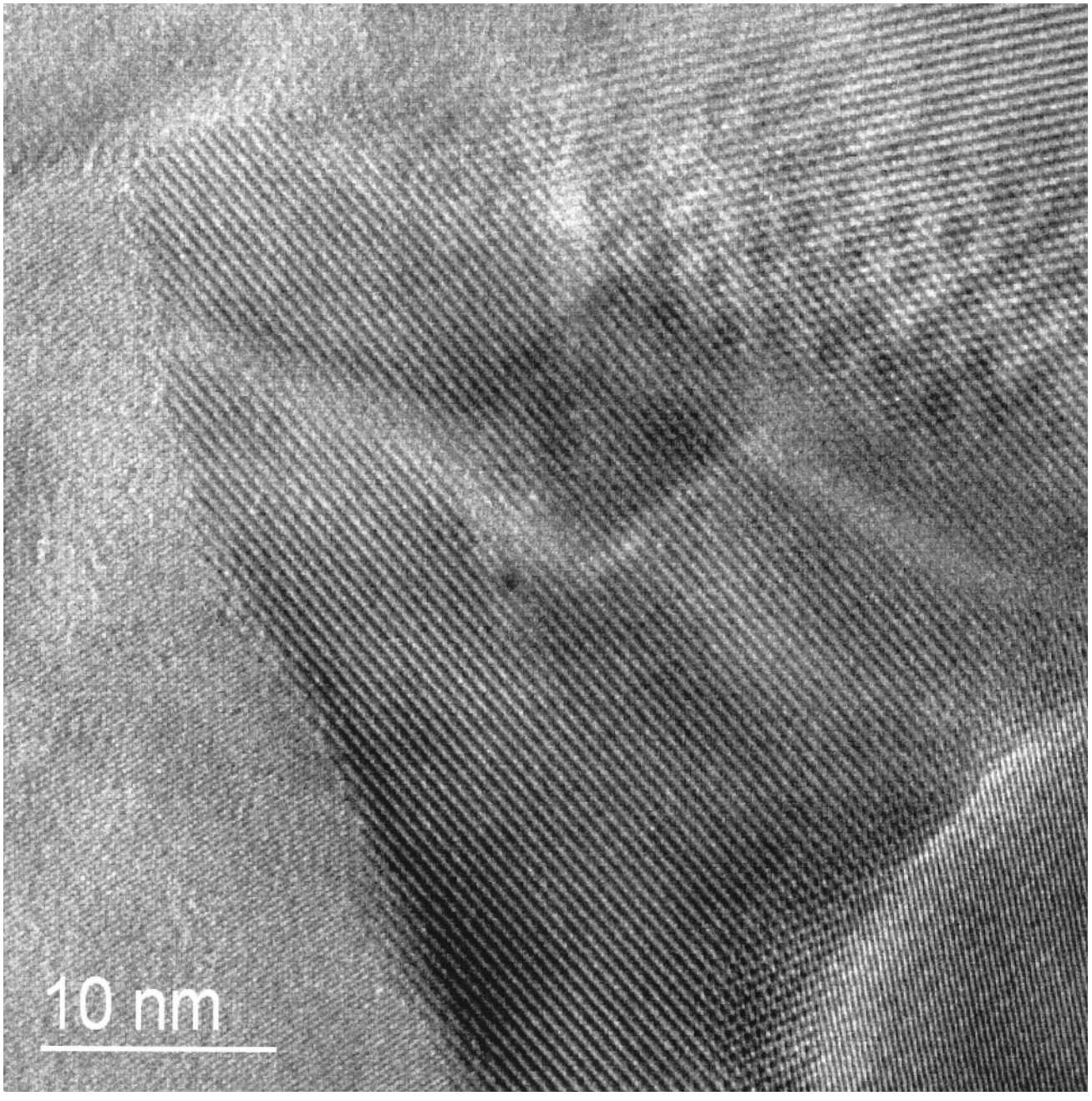

Fig. 7. HR-TEM micrograph of crystal phases present at a hematite surface in the presence of sulfate-reducing bacteria following 3 months of incubation. Several crystals are visible with regions of overgrowth in between. D-spacings of 2.6, 3.8 and 5.1 Å were consistently measured for the crystal phases at the surface.

polysulfides (for example Berner, 1970; Schoonen and Barnes, 1991a,b; Wilkin and Barnes, 1996; Benning et al., 2000). Thus, the apparent stoichiometric differences in ferrous sulfides produced could arise either from reduced pS^{2-}, or from the generation of an extremely reducing environment at the mineral surface in the presence of SRB. Since XPS indicates that precipitates formed at the hematite surface upon addition of H_2S in the absence of bacteria had equivalent E_b to those formed in the presence of SRB we conclude that pS^{2-} may exert more influence over formation of a particular phase than E_h, although we should not discount the potential control of E_h completely. Assessment of pFe^{2+} is not trivial. Metal ions are likely to interact with bacterial membranes (Fein et al., 1997), and extracellular polymers (Geesey and Jang, 1989; Barker and Banfield, 1996), both phenomena are likely to reduce the availability of free ferrous ions within bacterial biofilms. With regard to pS^{2-}, we are currently attempting to assess sulfide concentrations at mineral surfaces employing microelectrodes.

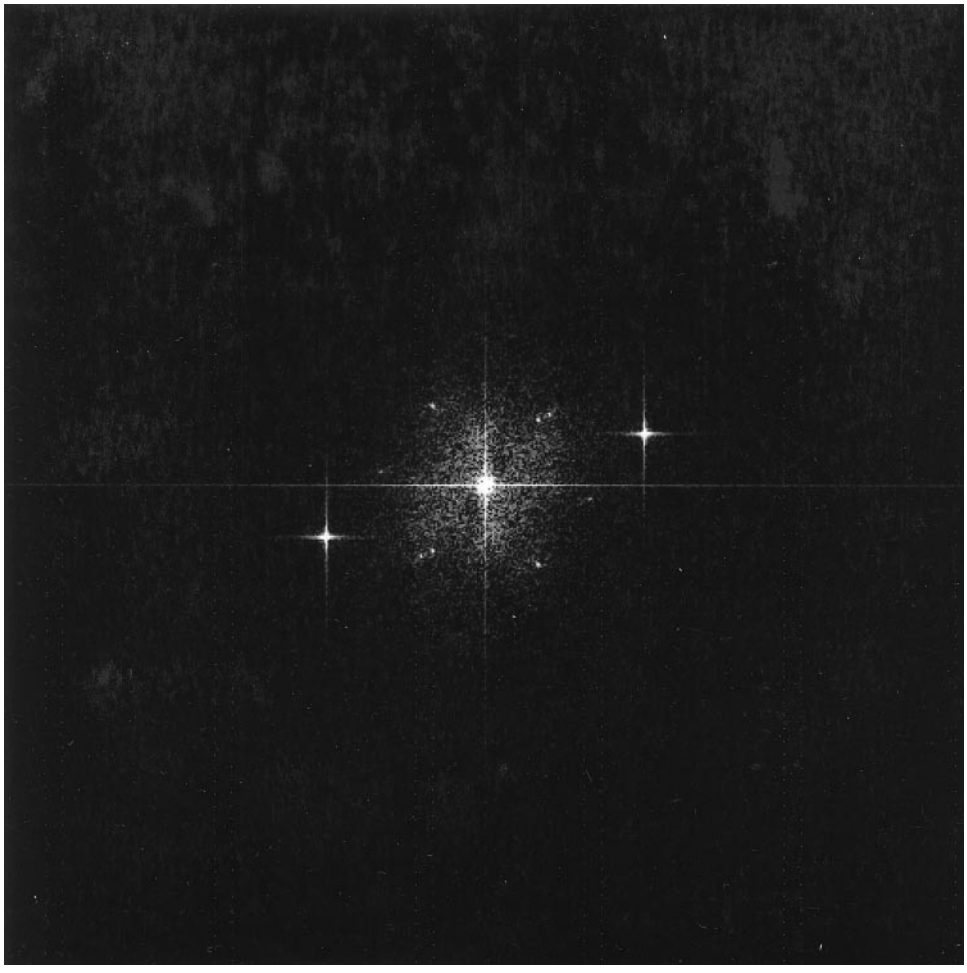

Fig. 8. Fourier transformation of the 5.1 Å lattice pattern in Figure 7 suggesting a hexagonal crystal structure.

4.2. Sulfur Species other than Fe-Sulfide Present at the Hematite Surface

Reductive dissolution of hematite by H_2S (Eqn. 2) is complex and although the products are often described as Fe-sulfide and elemental sulfur there are in fact many intermediates. Studies show these to include S_n^{2-}, SO_3^{2-}, SO_4^{2-} and $S_2O_3^{2-}$ (Pyzik and Sommer, 1981; dos Santos Afonso and Stumm, 1992; Davydov et al., 1998; Herszage and dos Santos Afonso, 2000) as well as S_8^0 (dos Santos Afonso and Stumm, 1992). Tetra- and pentasulfides are likely to be the only stable polysulfides in the culture medium (Giggenbach, 1972). Hematite dissolution is surface-controlled, the rate dependent upon the concentration of reductant(s) at the surface. Surface complexation models (Yates et al., 1974; Sulzberger et al., 1989) point to the significance of surface functional groups in mineral dissolution. Specifically for hematite, dos Santos Afonso and Stumm (1992) postulate the formation of FeS^- and FeSH surface complexes by exchange of O^{2-} for S^{2-} and SH^-, these new surface groups would then undergo electron transfer. The existence of SH^- groups at the hematite surface has been confirmed using FTIR spectroscopy (Davydov et al., 1998). Since Fe^{2+}-O^{2-} bonds in the hematite lattice are weakened in the process, $Fe^{2+}_{(aq.)}$ is released from the surface.

XPS spectra of all the hematite surfaces exposed to H_2S-practicing SRB revealed the presence of SO_3^{2-} and SO_4^{2-} as well as S_n^{2-}, at no time were peaks indicative of S_8^0 or thiosulfate observed. However, on the two hematite surfaces not exposed to H_2S, i.e., the surface exposed only to Lactate medium C in the absence of SRB and the surface exposed to Essex 6 growing in the absence of medium-SO_4^{2-}, peaks consistent with S_8^0 and $S_2O_3^{2-}$ were observed coincident with surface associated SO_4^{2-}. Reduction of hematite by H_2S (or Fe-sulfide, Tiller and Booth, 1962) precludes the accumulation of elemental sulfur and thiosulfate at the surface. A likely explanation is the reaction between elemental sulfur and sulfhydryl ions (HS^-) forming polysulfides (Teder 1971). At the same time both $S_2O_3^{2-}$ and SO_3^{2-} may disproportionate to SO_4^{2-} (Jørgensen, 1990; Canfield and Thamdrup, 1994; Habicht et al., 1998).

4.3. Implications of Pyrrhotite and Polysulfide Formation at Iron Oxide Surfaces

Iron sulfides have an important role to play in both the sulfur and iron cycles (Lovley, 1993; Nealson and Saffarini, 1994). The final product of iron sulfide formation, pyrite (FeS_2) (Rickard, 1969b; Berner, 1970; Berner, 1984), is stable (Lennie and

Vaughan 1996), although even pyrite is susceptible to dissolution by the Fe-oxidizers *Thiobacillus ferrooxidans* and *Leptospirillum ferrooxidans* (Bennett and Tributsch, 1978; Crundwell, 1996; Edwards et al., 1998). Intermediate species, i.e., mackinawite and greigite, being metastable at low temperatures (Lennie and Vaughan, 1996) are therefore likely to have an important influence upon the iron and sulfur balance. Fluctuations in ambient [Fe^{2+}] or [S^{2-}] (Anderko and Shuler 1997), pH (Brookins, 1988; Anderko and Shluer, 1997) or oxidation (Morse, 1991; Holmes, 1999) are likely to result in dissolution of sulfide precipitates. Such potential dissolution attains greater significance when one considers that other, potentially toxic, elements are often co-precipitated with Fe (Miller, 1950). The formation of pyrrhotite, a species considered stable at low temperatures (Kissin and Scott, 1982), will greatly limit the dissolution of Fe, S and other co-precipitates caused by environmental fluctuations in Fe, S and O_2. Polysulfides, being reduced species, represent a reactive form of elemental sulfur and together with monosulfides are responsible for maintaining trace metal concentrations in anoxic sediments at relatively high concentrations (Brooks et al., 1968; Presley et al., 1972).

Potential pyrrhotite formation by SRB also has implications for paleomagnetic studies of geomagnetic field behavior (Laj et al., 1991; Tauxe, 1993). Ferrous sulfide formation results in part from the dissolution of iron oxide minerals, thus the relative amounts of diagenetic ferrimagnetic minerals (i.e., pyrrhotite and greigite) compared to authigenic ferrimagnetic minerals (i.e., magnetite) are important considerations for the interpretation of paleomagnetic records. Roberts and Turner (1993) have identified pyrrhotite, together with greigite, associated with recent fine-grained sediments. They conclude that these phases exist as a result of interrupted sulfidation of precursor ferrous sulfides (i.e., arrested pyritization) due to low permeability of fine-grained sediments. Our results suggest that low sediment permeability need not be required for pyrrhotite formation but that low sulfide activity due to sulfide autooxidation at iron oxide surfaces may also result in pyrrhotite formation.

Thus, the presence of SRB at a hematite surface results in mineral dissolution and the formation of the stable iron sulfide pyrrhotite and reactive polysulfides resultant from excess H_2S production. Such a mechanism is consistent with observations by Morse and Cornwell (1987) that iron sulfides may exist principally as scales upon other minerals in sediments. Sulfide/polysulfide formation by SRB has the potential to greatly affect S, Fe and other trace metal concentrations in anoxic soils and sediments, of significance not only to the S and Fe cycles but also to the bioavailability of toxic trace metals and paleomagnetism.

Acknowledgments—XPS was performed at the Interfacial Chemical Analysis Laboratory at Montana State University. This research was supported by the Office of Biologic and Environmental Research, U. S. Department of Energy as part of the Natural and Accelerated Bioremediation Research Program (grant # ER 62630-3339). A portion of this work was performed at the Environmental Molecular Sciences Laboratory, a national scientific user facility sponsored by the Energy's Office of Biological and Environmental Research (OBER) and Pacific Northwest National Laboratory. This research was also supported by the OBER Natural and Accelerated Bioremediation Research Program. The authors are grateful to three anonymous reviewers whose thoughtful comments greatly improved the original manuscript.

Associate editor: D. J. Wesolowski

REFERENCES

Anderko A. and Shuler P. J. (1997) A computational approach to predicting the formation of iron sulfide species using stability diagrams. *Comput. Geosci.* **23,** 647–658.

Appelo C. A. J. and Postma D. (1996) Geochemistry, groundwater and pollution. A. A. Balkema, Rotterdam.

Asami K., Hashimoto K., and Shimodaira S. (1976) X-ray photoelectron spectrum of Fe^{2+} state in iron oxides. *Corrosion Sci.* **16,** 35–45.

Bacon P. B., Brewer P. G., Spencer D. W., Murray J. W., and Goddard J. (1980) Lead-210, polonium-210, manganese and iron in the Cariaco Trench. *Deep-Sea Res.* **27A,** 119–135.

Barker W. W. and Banfield J. F. (1996) Biologically versus inorganically mediated weathering reactions: Relationships between minerals and extracellular microbial polymers in lithobiontic communities. *Chem. Geol.* **132,** 55–69.

Baross J. A. and Deming J. W. (1983) Growth of 'black smoker' bacteria at temperatures of at least 250°C. *Nature* **303,** 423–426.

Bennett J. C. and Tributsch H. (1978) Bacterial leaching patterns on pyrite crystal surfaces. *J. Bacteriol.* **134,** 310–317.

Benning L. G., Wilkin R. T., and Konhauser K. O. (1999) Iron monosulphide stability: Experiments with sulphate reducing bacteria. In *Geochemistry of the Earth's Surface* (ed. H. Ármannsson) pp. 429–432. A. A. Balkema, Rotterdam.

Benning L. G., Wilkin R. T., and Barnes H. L. (2000). Reaction pathways in the Fe-S system below 100°C. *Chem. Geol.* **167,** 25–51.

Berner R. A. (1964) Iron sulfides formed from aqueous solutions at low temperatures and pressures. *J. Geol.* **72,** 293–306.

Berner R. A. (1970) Sedimentary pyrite formation. *Am. J. Sci.* **268,** 1–23.

Berner R. A. (1971) Principles of chemical sedimentology. McGraw-Hill, New York.

Berner R. A. (1982) Burial of organic carbon and pyrite sulfur in the modern ocean: Its geochemical and environmental significance. *Am. J. Sci.* **278,** 451–473.

Berner R. A. (1984) Sedimentary pyrite formation: An update. *Geochim. Cosmochim. Acta* **48,** 605–615.

Brookins D. G. (1988) Eh-pH Diagrams for Geochemistry. Springer-Verlag, New York.

Brooks R. R., Presley B. J., and Kaplan I. R. (1968) Trace elements in interstitial waters of marine sediments. *Geochim. Cosmochim. Acta* **32,** 397–414.

Brown G. E., Henrich V. E., Casey W. H., Clark D. L., Eggleston C., Felmy A., Goodman D. W., Grätzel M., Maciel G., McCarthy M. I., Nealson K. H., Sverjensky D. A., Toney M. F., and Zachara J. M. (1999) Metal oxide surfaces and their interactions with aqueous solutions and microbial organisms. *Chem. Rev.* **99,** 77–174.

Buckley A. N. and Woods R. (1985) X-ray photoelectron spectroscopy of oxidized pyrrhotite surfaces. I. Exposure to air. *Appl. Surf. Sci.* **22/23,** 280–287.

Buckley A. N. and Woods R. (1987) The surface oxidation of pyrite. *Appl. Surf. Sci.* **27,** 437–452.

Butlin K. R., Adams M. E., and Thomas M. (1949) The isolation and cultivation of sulphate-reducing bacteria. *J. Gen. Microbiol.* **3,** 49–59.

Byrne R. H. and Kester D. R. (1976) Solubility of hydrous ferric oxide and iron speciation in seawater. *Mar. Chem.* **4,** 255–274.

Canfield D. E. and Thamdrup B. (1994) The production of ^{34}S-depleted sulfide during bacterial disproportionation of elemental sulfur. *Science* **266,** 1973–1975.

Cormack B. P., Valdivia R. H., and Falkow S. (1996) FACS-optimized mutants of the green fluorescent protein (GFP). *Gene* **173,** 33–38.

Costerton J. W., Lewandowski Z., Caldwell D. E., Korber D. R., and Lappin-Scott H. M. (1995) Bacterial biofilms. *Ann. Rev. Microbiol.* **49,** 711–745.

Davydov A., Chaung K. T., and Sanger A. R. (1998) Mechanism of H_2S oxidation by ferric oxide and hydroxide surfaces. *J. Phys. Chem. B.* **102,** 4745–4752.

DeLong E. F., Frankel R. B., and Bazylinski D. A. (1993) Multiple evolutionary origins of magnetotaxis in bacteria. *Science.* **259,** 803–806.

Donald R. and Southam G. (1999) Low temperature anaerobic bacterial diagenesis of ferrous monosulfide to pyrite. *Geochim. Cosmochim. Acta* **63,** 2019–2023.

Edwards K. J., Schrenk M. O., Hamers R., and Banfield J. F. (1998)

Microbial oxidation of pyrite: Experiments using microorganisms from an extreme acidic environment. *Am. Mineral.* **83,** 1444–1453.
Errampalli D., Leung K., Cassidy M. B., Kostrzynska M., Blears M., Lee H., and Trevors J. T. (1999) Applications of the green fluorescent protein as a molecular marker in environmental organisms. *J. Microbiol. Methods* **35,** 187–199.
Fein J. B., Daughney C. J., Yee N. and Davis T. A. (1997) A chemical equilibrium model for metal adsorption onto bacterial surfaces. *Geochim. Cosmochim. Acta* **61,** 3319–3328.
Frankel R. B., Bazylinski D. A., and Schüler D. (1998) Biomineralization of magnetic iron minerals in bacteria. *Supramolec. Sci.* **5,** 383–390.
Geesey G. G. and Jang L. (1989) Interactions between metal ions and capsular exopolymers. In *Metal ions and Bacteria* (eds. T. J. Beveridge and R. J. Doyle) Chap. 11, pp. 325–357. Wiley-Interscience.
Ghiorse W. C. and Wilson J. T. (1988) Microbial ecology of the terrestrial subsurface. *Adv. Appl. Microbiol.* **33,** 107–172.
Giggenbach W. (1972) Optical spectra and equilibrium distribution of polysulfide ions in aqueous solution at 20°C. *Inorg. Chem.* **11,** 1201–1207.
Goldhaber M. B. and Kaplan I. R. (1974) The sulfur cycle. In *The Sea—Ideas and Observations on Progress in the Study of the Seas* (ed. E. D. Goldberg). pp. 569–655. Wiley Interscience.
Gupta R. P. and Sen S. K. (1974) Calculation of multiplet structure of core *p*-vacancy levels. *Phys. Rev. B* **10,** 71–77.
Gupta R. P. and Sen S. K. (1975) Calculation of multiplet structure of core *p*-vacancy levels. II. *Phys. Rev. B* **12,** 15–19.
Habicht K. S., Canfield D. E., and Rethmeier J. (1998) Sulfur isotope fractionation during bacterial reduction and disproportionation of thiosulfate and sulfite. *Geochim. Cosmochim. Acta* **62,** 2585–2595.
Hamilton, W. A. (1991) Sulphate-reducing bacteria and their role in microbially influenced corrosion. In *Microbially influenced corrosion and biodeterioration* (ed. N. J. Dowling et al.). pp. i–iv. Institute for Applied Microbiology.
Harvey R. W., Smith R. L., and George L. (1984) Effect of organic contamination upon microbial distribution and heterotrophic uptake in a Cape Cod, Mass., aquifer. *Appl. Environ. Microbiol.* **48,** 1197–1202.
Herbert R. B., Benner S. G., Pratt A. R., and Blowes D. W. (1998) Surface chemistry and morphology of poorly crystalline iron sulfides precipitated in media containing sulfate-reducing bacteria. *Chem. Geol.* **144,** 87–97.
Herszage J. and dos Santos Afonso M. (2000). The autooxidation of hydrogen sulfide in the presence of hematite. *Colloids Surf. A* **168,** 61–69.
Holmes J. (1999) Fate of incorporated metals during mackinawite oxidation in sea water. *Appl. Geochem.* **14,** 277–281.
Horng C. S., Torii M., Shea K. S., and Kao S. J. (1998) Inconsistent magnetic polarities between greigite- and pyrrhotite/magnetite-bearing marine sediments from the Tsailiano-chi section, southwestern Taiwan. *Earth Planet. Sci. Lett.* **164,** 467–481.
Hyland H. M. and Bancroft G. M. (1989) An XPS study of gold deposition at low temperatures on sulphide minerals: Reducing agents. *Geochim. Cosmochim. Acta* **53,** 367–372.
Jesior J. C. (1986) How to avoid compression. *J. Ultrastruc. Mol. Struc. Res.* **95,** 210–217.
Jones C. F., Lecount S., Smart R. St. C., and White T. (1992) Compositional and structural alteration of pyrrhotite surfaces in solution: XPS and XRD studies. *Appl. Surf. Sci.* **55,** 65–85.
Jørgensen B. B. (1977) The sulfur cycle of a coastal marine sediment (Limfjorden, Denmark). *Limnol. Oceanogr.* **22,** 814–831.
Jørgensen B. B. (1990) A thiosulfate shunt in the sulfur cycle of marine sediments. *Science* **249,** 152–154.
Junta-Rosso J. L. and Hochella M. F. (1996) The chemistry of hematite {001} surfaces. *Am. Mineral.* **60,** 305–314.
Kissin S. A. and Scott S. D. (1982) Phase relations involving pyrrhotite below 350°C. *Econ. Geol.* **77,** 1739–1754.
Kobayashi K. and Nomura M. (1972) Iron sulfides in the sediment cores from the Sea of Japan and their geophysical implications. *Earth Planet. Sci. Lett.* **16,** 200–208.
Laj C., Mazaud A., Weeks R., Fuller M., and Herrero-Bervera E. (1991) Geomagnetic reversal paths. *Nature* **351,** 447.
Le Gall J., Payne W. J., Chen L., Liu M. Y., and Xavier A. V. (1994) Localization and specificity of cytochromes and other electron transfer proteins from sulfate-reducing bacteria. *Biochimie* **76,** 655–665.
Lennie A. R., Redfern S. A. T., Schofield P. F., and Vaughan D. J. (1995a) Synthesis and Rietveld crystal structure refinement of mackinawite, tetragonal FeS. *Mineral. Mag.* **59,** 677–683.
Lennie A. R., England K. E. R., and Vaughan D. J. (1995b) Transformation of synthetic mackinawite to hexagonal pyrrhotite: A kinetic study. *Am. Mineral.* **80,** 960–967.
Lennie A. R. and Vaughan D. J. (1996) Spectroscopic studies of iron sulfide formation and phase relations at low temperatures. In *Mineral Spectroscopy: A Tribute to Roger G. Burns* (ed. M. D. Dyar et al.). pp. 117–131. The Goechemical Society (Special Publication No. 5).
Lord C. J. and Church T. M. (1983) The geochemistry of salt marshes: Sedimentary ion diffusion, sulfate reduction, and pyritization. *Geochim. Cosmochim. Acta* **47,** 1381–1391.
Lovley D. R. (1993) Dissimilatory metal reduction. *Ann. Rev. Microbiol.* **47,** 263–290.
Luther G. W. III (1991) Pyrite synthesis via polysulfide compounds. *Geochim. Cosmochim. Acta* **55,** 2839–2849.
Magee E. L., Ensley B. D., and Barton L. L. (1978) An assessment of growth yields and energy coupling in *Desulfovibrio. Arch. Microbiol.* **117,** 21–26.
Manocha A. S. and Park R. L. (1977) Flotation related ESCA studies on PbS surfaces. *Appl. Surface Sci.* **1,** 129–141.
Matthysse A. G., Stretton S., Dandie C., McClure N. C., and Goodman A. E. (1996) Construction of GFP vectors for use in Gram-negative bacteria other than *Escherichia coli. FEMS Microbiol. Lett.* **145,** 87–94.
McIntyre N. S. and Zetaruk D. G. (1977) X-ray photoelectron spectroscopic studies of iron oxides. *Anal. Chem.* **49,** 1521–1529.
Meyer F. H., Riggs O. L., McGlasson R. L., and Sudbury J. D. (1958) Corrosion products of mild steel in hydrogen sulfide environments. *Corrosion* **14,** 69–75.
Miller L. P. (1950) Formation of metal sulfides through the activities of sulfate-reducing bacteria. *Contr. Boyce Thompson Inst. Plant Res.* **16,** 85–89.
Morse J. W. (1991) Oxidation kinetics of sedimentary pyrite in seawater. *Geochim. Cosmochim. Acta* **55,** 3665–3667.
Morse J. W. and Cornwell, J. C. (1987) Analysis and distribution of iron sulfide minerals in recent anoxic marine sediments. *Mar. Chem.* **22,** 55–69.
Mycroft J. R., Bancroft G. M., McIntyre N. S., Lorimer J. W., and Hill I. R. (1990) Detection of sulphur and polysulphides on electrochemically oxidized pyrite surfaces by X-ray photoelectron spectroscopy and Raman spectroscopy. *J. Electroanal. Chem.* **292,** 139–152.
Nealson K. H. and Saffarini D. (1994) Iron and Manganese in anaerobic respiration: Environmental significance, physiology, and regulation. *Ann. Rev. Microbiol.* **48,** 311–343.
Olson G. J., Dockins W. S., McFeters G. A. and Inverson W. P. (1981) Sulfate-reducing and methanogenic bacteria from deep aquifers in Montana. *Geomicrobiol. J.* **2,** 327–340.
Pósfai M., Buseck P. R., Bazylinski D. A., and Frankel R. B. (1998) Iron sulfides from magnetotactic bacteria: Structure, composition and transitions. *Am. Mineral.* **83,** 1469–1481.
Postgate J. R. (1963) Versatile medium for the enumeration of sulfate-reducing bacteria. *Appl. Microbiol.* **11,** 265–267.
Postgate J. R. and Campbell L. L. (1966) Classification of *Desulfovibrio* species, the nonsporulating sulfate-reducing bacteria. *Bacteriol. Rev.* **30,** 732–738.
Pratt A. R., Muir I. J., and Nesbitt H. W. (1994a) X-ray photoelectron and Auger electron spectroscopic studies of pyrrhotite and mechanism of air oxidation. *Geochim. Cosmochim. Acta* **58,** 827–841.
Pratt A. R., Nesbitt H. W. and Muir I. J. (1994b) Generation of acids from mine waste: Oxidative leaching of pyrrhotite in dilute H_2SO_4 solutions at pH 3.0. *Geochim. Cosmochim. Acta* **58,** 5147–5159.
Presley B. J., Kolodny Y., Nissenbaum A., and Kaplan I. R. (1972) Early diagenesis in a reducing fjord, Saanich Inlet, Br. Colombia, II. Trace element distribution in interstitial water and sediments. *Geochim. Cosmochim. Acta* **36,** 1073–1090.
Pyzik A. J. and Sommer S. E. (1981) Sedimentary iron monosulfides: Kinetics and mechanism of formation. *Geochim. Cosmochim. Acta* **45,** 687–698.

Rickard D. T. (1969a) The microbiological formation of iron sulphides. *Stokholm Contrib. Geol.* **20,** 49–66.

Rickard D. T. (1969b) The chemistry of iron sulphide formation at low temperatures. *Stokholm Contrib. Geol.* **20,** 67–95.

Ringas C. and Robinson F. P. A. (1988) Corrosion of stainless steel by sulfate-reducing bacteria—electrochemical techniques. *Corrosion* **44,** 391–396.

Robert M. and Berthelin J. (1986) Role of biological and biochemical factors in soil mineral weathering. In *Interactions of soil minerals with natural organics and microbes* (ed. P. M. Huang and M. Schnitzer). Chap. 12, pp. 453–495. Soil Science Society of America, Madison, WI. (Special Publication No. 17).

Roberts A. P. and Turner G. M. (1993) Diagenetic formation of ferrimagnetic iron sulfide minerals in rapidly deposited marine sediments, South Island, New Zealand. *Earth Planet. Sci. Lett.* **115,** 257–273.

Rouxhet P. G. and Genet M. J. (1991) Chemical composition of the microbial cell surface by X-ray photoelectron spectroscopy. In *Microbial Cell Surface Analysis. Structural and Physiochemical Methods* (ed. N. Mozes et al.). Chap. 8, pp. 173–220. VCH Publications Inc., Baton Rouge.

dos Santos Afonso M. and Stumm W. (1992) Reductive dissolution of iron(III) (hydr)oxides by hydrogen sulfide. *Langmuir* **8,** 1671–1675.

Schoonen M. A. A. and Barnes H. L. (1991a) Reactions forming pyrite and marcasite from solution: I. Nucleation of FeS_2 below 100°C. *Geochim. Cosmochim. Acta* **55,** 1495–1504.

Schoonen M. A. A. and Barnes H. L. (1991b) Reactions forming pyrite and marcasite from solution: II. Via FeS_2 precursors below 100°C. *Geochim. Cosmochim. Acta* **55,** 1505–1514.

Schüler D. and Frankel R. B. (1999) Bacterial magnetosomes: Microbiology, biomineralization and biotechnological applications. *Appl. Microbiol. Biotechnol.* **52,** 464–473.

Shirley D. A. (1972) High-resolution X-ray photoemission spectrum of the valence bands of gold. *Phys. Rev. B* **5,** 4709–4714.

Smith A. D. and Klug M. J. (1981) Electron donors utilized by sulfate-reducing bacteria in eutrophic lake sediments. *Appl. Env. Microbiol.* **42,** 116–121.

Sulzberger B., Suter D., Siffert C., and Banwart S. (1989) Dissolution of Fe(III) (hydr)oxides in natural waters: Laboratory assessment of the kinetics controlled by surface coordination. *Mar. Chem.* **28,** 127–144.

Sweeney R. E. and Kaplan I. R. (1973) Pyrite framboid formation: laboratory synthesis and marine sediments. *Econ. Geol.* **68,** 618–634.

Tauxe L. (1993) Sedimentary records of relative paleointensity of the geomagnetic field: Theory and practice. *Rev. Geophys.* **31,** 319–354.

Taylor P., Rummery T. E., and Owen D. G. (1979) On the conversion of mackinawite to greigite. *J. Inorg. Nucl. Chem.* **41,** 595–596.

Teder A. (1971) The equilibrium between elementary sulfur and aqueous polysulfide solutions. *Acta Chem. Scand.* **25,** 1722–1728.

Thauer, R. K., Jungermann, K., and Decker, K. (1977) Energy conservation in chemotrophic anaerobic bacteria. *Bacteriol. Rev.* **41,** 100–180.

Tiller A. K. and Booth G. H. (1962) Polarization studies of mild steel in cultures of sulfate-reducing bacteria. II. Thermophilic organisms. *Trans. Faraday Soc.* **58,** 110–115.

Vaughan D. J. and Ridout M. S. (1971) Mössbauer studies of some sulfide minerals. *J. Inorg. Chem.* **33,** 741–746.

Wagner C. D., Riggs W. M., Davies L. E., Moulder J. F., and Mailenberg G. M. (1992) Handbook of X-ray photoelectron spectroscopy. Perkin-Elmer.

Wall J. D., Rapp-Giles B. J., and Rousset M. (1993) Characterization of a small plasmid from *Desulfovibrio desulfuricans* and its use for shuttle vector construction. *J. Bacteriol.* **175,** 4121–4128.

Webb, J. S., McGinness, S., and Lappin-Scott, H. M. (1998) Metal removal by sulfate-reducing bacteria from natural and constructed wetlands. *J. Appl. Microbiol.* **84,** 240–248.

Wilkin R. T. and Barnes H. L. (1996) Pyrite formation by reactions of iron monosulfides with dissolved inorganic and organic sulfur species. *Geochim. Cosmochim. Acta* **60,** 4167–4179.

Yates D. E., Levine S., and Healy T. (1974) Site-binding model of the electrical double layer at the oxide/water interface. *J. Chem. Soc., Faraday Trans. 1.* **70,** 1807–1818.